Sensors and Materials, Vol. 28, No. 3 (2016) 191–199
MYU Tokyo

S & M 1169

Particle Size Determination and Magnetic Characterization of Fe_3O_4 Nanoparticles Using Superconducting Quantum Interference Device Magnetometry

Vineet Kumar,[1,2] Rabindra Prasad Singh,[3] Satish Kumar,[4]
Avinash Agarwal,[2] and Praveen Singh[1*]

[1]Biophysics Section, Division of Veterinary Biotechnology, Indian Veterinary Research Institute, Izatnagar, Bareilly 243122, U.P., India
[2]Physics Department, Bareilly College, Bareilly 243001, U.P., India
[3]Division of Biological Products, Indian Veterinary Research Institute, Izatnagar, Bareilly 243122, U.P., India
[4]Division of Veterinary Biotechnology, Indian Veterinary Research Institute, Izatnagar, Bareilly 243122, U.P., India

(Received December 31, 2015; accepted March 1, 2016)

Keywords: magnetite, monodisperse, nanoparticle, superparamagnetic, superconducting quantum interference device

Magnetic nanoparticles (MNPs) were synthesized by a chemical co-precipitation method, which produces monodisperse, nanosize, benign superparamagetic iron oxide nanoparticles (SPIONs) at a reduced synthesis temperature. The crystal structure, morphology, and magnetic characterization were determined by X-ray diffraction (XRD), transmission electron microscopy (TEM), and superconducting quantum interference device (SQUID) magnetometer, respectively. The XRD pattern shows that the presence of the most intense peak corresponds to the (311) crystallographic orientation of the spinel phase of Fe_3O_4 MNPs. The crystallite size of 4–6 nm was determined from the XRD pattern by using the Scherrer approximation. A TEM image of the MNP showed the mean diameter of 18 ± 10 nm. Magnetization versus temperature (*M–T*) curve values were used to determine the blocking temperature and particle size by Néel–Arrhenius law and magnetization versus magnetic field (*M–H*) curve values were used to calculate the size of magnetic particles by the Langevin equation. The particle sizes were found to be 19 and 10 nm. The MNPs proved to be superparamagnetic by *M–H* characterization at 10 and 300 K. The saturation magnetizations of 57.54 and 8.38 emu/gm were obtained for Fe_3O_4 MNPs and bovine serum albumin (BSA)-capped Fe_3O_4 MNPs, respectively. The blocking temperatures of 150 and 130 K were observed for Fe_3O_4 MNPs and BSA-capped Fe_3O_4 MNPs, respectively. The SPIONs reported in this study vividly demonstrated their suitability for tagging biomolecules and their potential for rapid immunoassay application.

1. Introduction

Magnetic nanoparticles (MNPs) have attracted great attention because of their unique physical and chemical properties and their potential in various biomedical applications, such as contrast

*Corresponding author: e-mail: psingh67@yahoo.com

ISSN 0914-4935

agents, carriers for drug delivery, the magnetic separation in microbiology, biochemical sensing,[1] deoxyribo nucleic acid (DNA) and ribo nucleic acid (RNA) purification, cell separation,[2–4] targeted drug delivery,[5,6] separation,[7] tissue repair,[8] cancer treatment through hyperthermia,[9,10] and magnetic resonance imaging (MRI) contrast enhancement.[11–13] MRI is an appealing non-invasive approach for early cancer diagnosis and therapeutics.[14] The colloidal magnetic particles are being used in delivery as carriers for site specific targeting of drugs.[15] Delivery materials are expected to bind a pharmaceutical drug on their surface that could be driven to the target organ and released there. The size, charge, and surface chemistry of the magnetic particles are very important parameters and strongly affect both the blood circulation time and the bioavailability of the particle within the body.[16,17]

There are various methods to prepare the MNPs of nanometer size range with varying properties depending upon their end uses. These MNPs have assumed a greater degree of research interest due to their immense technological applications in labeling[18] and sensing applications. The bioconjugation and biolabeling of Fe_3O_4 nanoparticles with biomolecules, ligands, drugs, and fluorescent dyes were accomplished by researchers[19] to make them multifunctional nanostructures for biomedical use. There is growing need for the fabrication of magnetic nanoshells for delivery applications[20] at tissue sites.[21] There are few reports of fabricating Fe_3O_4 MNPs for biosensing and detection applications by superconducting quantum interference device (SQUID) magnetometry[10] and utilizing the magnetic data values for determination of the size of nanoparticles precisely. In the present work, aqueous, monodisperse, stable, and biocompatible Fe_3O_4 MNPs have been synthesized by the ammonia precipitation method to obtain nanosized superparamagnetic iron oxide nanoparticles (SPIONs). The SPIONs were activated, characterized and functionalized with bovine serum albumin (BSA) as a model to see its conjugation for their tailor-made application as a detection probe. Efforts have also been made to deduce the size of MNPs from SQUID magnetometer data. For comparison with data obtained, measurement of size of nanoparticles on transmission electron microscopy (TEM) was made.

2. Experimental

2.1 Methods

Ferric chloride ($FeCl_3$, MP Biomedicals Ltd.), ferrous chloride ($FeCl_2{\cdot}4H_2O$, MP Biomedicals Ltd.), ethanol (99%), ammonia (NH_3, about 25% 0.91 Pure, Merck), hydrogen chloride (HCl, 99.9%, S.D. Fine-Chem Ltd.), and deionized water (S.D. Fine-Chem Ltd.) were used as received. MNPs were initially activated with triethoxy-silane (3-aminopropyl, 98%, Sigma-Aldrich). The protein conjugations were achieved using carbodiimide chemistry, wherein *N*-hydroxy succinimide (97%, Sisco Research Laboratories Pvt., Ltd., India), *N*-ethylcarbodiimide hydrochoride ($C_8H_{17}N_3HCl$, Sisco Research Laboratories Pvt., Ltd., India) and BSA (98%, Amresco, USA) were used.

X-ray diffraction (XRD) patterns were recorded on a Philips Diffractometer (Philips, X´Pert PW 3040 PAN Analytical, Netherlands) available at the Textile Engineering Department, Indian Institute of Technology (ITT) Delhi, New Delhi. The powder XRD patterns of MNPs were recorded in 2θ range from 10 to 70°, at a scan rate of 2°/min. A transmission electron microscope (JEM1011, Jeol, Japan) was used at GB Pant University of Agriculture and Technology, Pantnagar. Magnetization studies were conducted over a system, Quanta Design, MP MSXL7, USA at SQUID National Facility, Department of Physics, IIT Delhi. *M–H* curves were measured at 300 and 10 K

and the maximum applied field was 30000 Oe with a loading rate of 100 Oe/s, where parameters including saturation magnetization (M_s) and coercive field (H) were evaluated.

2.2 Preparations of stock solutions

2 M HCl (21 ml of concentrated hydrochloric acid in 250 ml water) was prepared for making iron solutions. 2 M $FeCl_2$ in 2 M HCl (39.76 g of $FeCl_2 \cdot 4H_2O$ in 100 ml of 2 M HCl) and 1 M $FeCl_3$ in 2 M HCl (67.58 g of $FeCl_3 \cdot 6H_2O$ or 40.55 g of $FeCl_3$ in 250 ml of 2 M HCl) were prepared for the synthesis of Fe_3O_4 MNPs. An aqueous NH_3 (200 ml of concentrated aqueous NH_3 diluted to 3 L with H_2O) was prepared for reducing the iron solutions.

2.3 Synthesis of monodisperse MNPs

1.0 ml of stock $FeCl_2$ solution and 4.0 ml of stock $FeCl_3$ solution are poured into a flask. Place a magnetic stirring bar in the flask and begin stirring vigorously. Add drop wise by pipette or burette 50 ml of 1 M aqueous NH_3 solution into the flask. We have found that a slow rate of addition is critical, and a pipette or burette is a convenient means of slowing the addition rate. Magnetite, a black precipitate, will form immediately. Stir throughout the addition of the ammonia solution. Cease stirring and allow the precipitate to settle (5–7 min) then decant and dispose of most of the liquid. Stir the remaining solution and centrifuge the solution for 2 min at 2000 rpm. In general, at least 15–20 ml of liquid should be centrifuged to obtain an adequate amount of solid magnetite for preparing a magnetite sample; one or more centrifuge tubes can be used for this step, depending on the centrifuge available. Decant the supernatant after centrifugation. The dark, sludge like solid at the bottom of the tube is magnetite. Magnetically stir the solution 6–7 times, and give three ethanol washes to remove excess ammonia from the solution. Gently pour the stirring bar and attached sludge into a plastic weighing boat. Then, the precipitate is incubated and dried at 45 °C for 48 h.

$$2FeCl_3 + FeCl_2 + 8NH_3 + 4H_2O \rightarrow Fe_3O_4 + 8NH_4Cl$$

2.4 Functionalization procedure of MNPs

0.5 g of the syntheiszed magnetite powder was washed in absolute ethanol and deionized water using an ultrasonicator. The aqueous content was decanted, dried, then mixed with 1 ml 3-aminopropyl triethoxy silane for incubation at room temperature for 18 h. Amine-group-coupled MNPs were washed with ethanol and dried. The protein attachment was accomplished through carbodiimide linking of the carboxylic group of the protein to the NH_2 group of the silane layer over the MNPs. The 0.1 M *N*-hydroxy succinimide, 0.4 M *N*-ethylcarbodiimide hydrochoride, and 1 mg/ml BSA were incubated for 30 min at room temperature.

The functionalization steps as shown in Fig. 1 were carried out at pH 7.2 in PBS prepared with 137 mM NaCl, 2.7 mM KCl, 4.3 mM Na_2HPO_4, and 1.4 mM KH_2PO_4.

3. Results and Discussion

Synthesized MNPs underwent morphological investigation by TEM as shown in Fig. 2. The mean size of a MNP is about 18 ± 10 nm. The MNPs are spherical and monodisperse in nature.

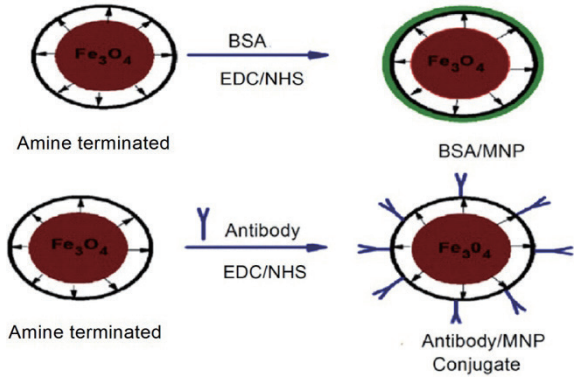

Fig. 1. (Color online) Conjugation mechanism of Fe_3O_4 MNPs with BSA and antibody.

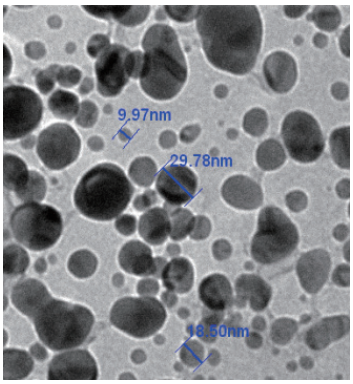

Fig. 2. (Color online) TEM of Fe_3O_4 MNPs.

The MNPs were further characterized by XRD for structural determination and estimation of crystallite size. The powder XRD pattern of the sample was recorded on a diffractometer (Philips, X´Pert PW 3040 PAN Analytical, Netherlands) using CuKα (1.5406 Å) radiation at room temperature in the range of 30° to 70° in the 2θ scale with a scanning step length of 2°/min. XRD can be used to characterize the crystallinity of nanoparticles as well as the mean diameter of MNPs. The XRD pattern was compared with the standard (JCPDF NO.79-0419 ICSD NO. 065341) and we confirmed the cubic spinel phase of magnetite as shown in Fig. 3. The peaks were indexed as planes (220), (311), (400), (511), and (440), which corresponds to a cubic unit cell, characteristic of a cubic spinel structure.[22–24] Therefore, it was confirmed that the crystalline structure of the obtained MNPs agreed with the structure of an inverse-spinel-type oxide. The crystallite size was determined from the full-width at half maximum (FWHM) of the strongest reflection of the (311) peak using the Scherrer approximation, which assumes the small crystallite size to be the cause of line broadening,

$$D = K\lambda/\beta\cos\theta. \quad (1)$$

Here, D is the mean crystallite size, K is a shape function, for which a value of 0.9 is used, λ is the wavelength (1.54 Å) of the radiation, β is the FWHM in radians in the 2θ scale, and θ is the Bragg angle. The crystallite size was calculated to be 4.42 ± 0.25 nm. Owing to the broad XRD pattern

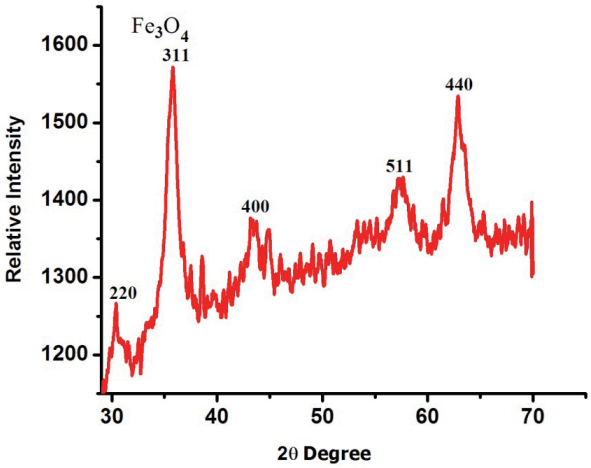

Fig. 3. (Color online) XRD pattern of Fe_3O_4 magnetite phase.

lines, it can be said that the MNPs have sizes of nanometers; therefore, it is established that MNPs were conveniently prepared by the modified co-precipitation process.

The *M–H* characterization of the Fe_3O_4 MNPs and BSA-capped Fe_3O_4 MNPs was carried out using a SQUID magnetometer (Quantum design, USA) at 10 and 300 K with a magnetic field from −30000 to 30000 Oe and a loading rate of 100 Oe/s, as shown in Fig. 4(a). The *M–H* observations proved that the SPIONs and BSA-capped SPIONs are superparamagnetic in nature at 10 and 300 K. The saturation magnetization for the Fe_3O_4 MNPs was measured to be 57.54 and 49.39 emu/gm at 10 and 300 K, respectively. However, the saturation magnetization for the BSA-capped Fe_3O_4 MNPs was observed to be 11.37 and 8.38 emu/gm at 10 and 300 K, respectively.

The saturation magnetization obtained for SPIONs was found to be lower than the bulk value of MNPs, 92 emu/gm.[25] Generally, smaller magnetite nanoparticles cause more chaotic motion and decrease in the magnetic moment. There is no remanance, and the coercivity is nearly zero. Magnetization (M_s) and applied field (H) can be described by the Langevin equation:[25,26]

$$M = M_s \coth(Y-1), \text{ where } Y = mH/KT \tag{2}$$

Here, M_s (= 49.39 emu/gm) is the saturation magnetization of the BSA-capped SPIONs at 300 K, K_B (= 1.3807×10^{-23} J/K) is the Boltzmann constant. The coercive field (H) depends on temperature, M is the specific magnetization above T_b, and m is the average magnetic moment of an individual nanoparticle in the sample and is calculated to be 1.3×10^{-19} emu at 300 K. Taking into account the density of magnetite of 5.046 g/cm^3, the diameter of a MNP is found to be 10 nm, which is in approximate agreement with TEM results. The saturation magnetization for the Fe_3O_4 SPIONs is observed to be 57.54 emu/g at 10 K, which declines to 49.34 emu/g at 300 K. However, for BSA-capped Fe_3O_4 SPIONs, M_s is observed to be 11.37 emu/g at 10 K, which is lowered to 8.38 emu/g owing to thermal agitations of the magnetic moments of nanoparticles. The remanance magnetization is 4.4 emu/g for the Fe_3O_4 SPIONs at a lower temperature of 10 K. The coercivity (H_c) is observed to be 201 Oe for the Fe_3O_4 SPIONs at 10 K, which increased to 256 Oe for the BSA-capped Fe_3O_4 SPIONs at 10 K (Table 1). The *M–H* hysteresis loops were observed for the

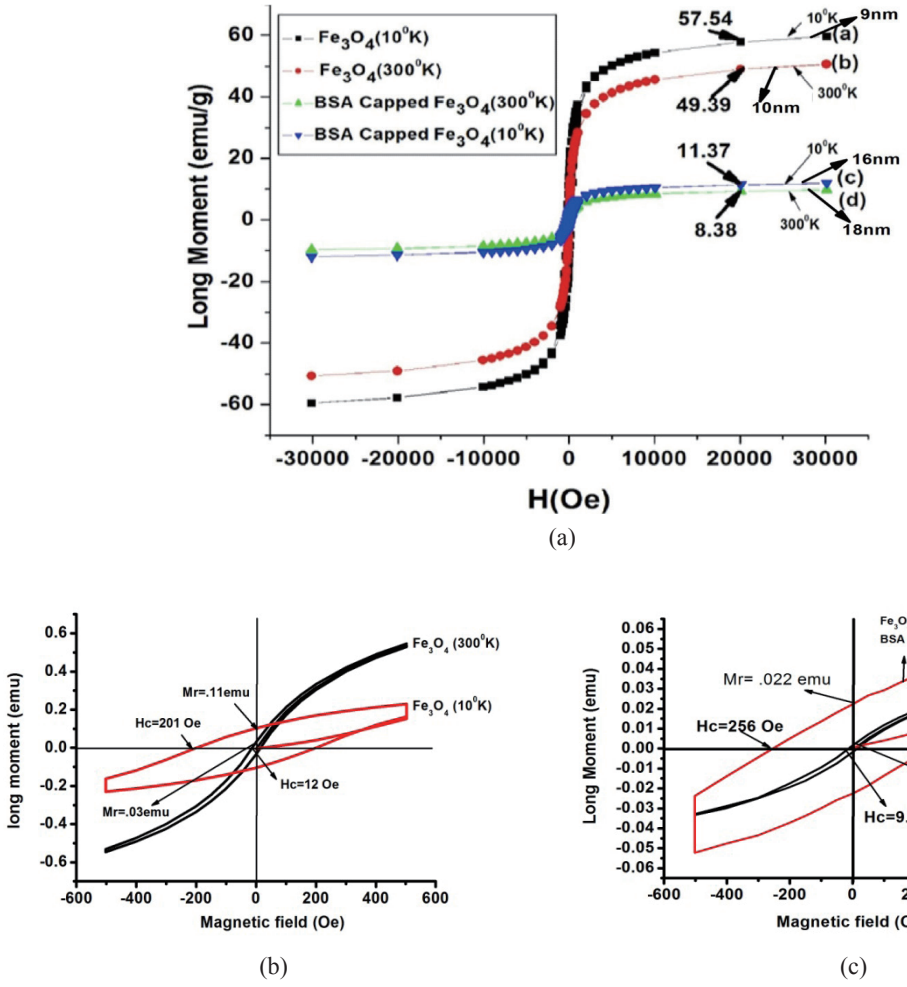

Fig. 4. (Color online) (a) *M–H* hysterises loop of Fe_3O_4 MNPs and BSA-capped Fe_3O_4 MNPs. (b) *M–H* hysterises loop of Fe_3O_4 MNPs at 10 and 300 K. (c) *M–H* hysterises loop of BSA-capped Fe_3O_4 MNPs at 10 and 300 K.

Table 1
Saturation magnetization (M_s), remanence magnetization (M_r), and coercivity (H_c) at temperatures of 10 and 300 K.

Sample	Saturation magnetization M_s (emu/gm)	Remanent magnetization M_r (emu/gm)	Coercivity H_c (Oe)
Fe_3O_4 (300 K)	49.39	1.2	12
Fe_3O_4 (300 K) BSA-capped	8.38	0.1	9.9
Fe_3O_4 (10 K)	57.54	4.4	201
Fe_3O_4 (10 K) BSA-capped	11.37	2.2	256

Fe_3O_4 SPIONs and BSA-capped Fe_3O_4 SPIONs at 10 and 300 K are depicted in Figs. 4(b) and 4(c), respectively. The magnetic properties of the MNPs have been believed to be highly dependent on the sample shape, crystallinity, and magnetic anisotropy. The hysteresis loop of the spherical Fe_3O_4 nanocrystallites at room temperature shows a ferromagnetic behaviour, as shown in Figs. 4(b) and 4(c). The saturation magnetization (M_s), remanant magnetization (M_r), coercivity (H_c) values are given in Table 1 for the SPION samples.

It is reported that one-dimensional nanostructures have both increased shape anisotropy and magnetocrystalline anisotropy, which exert influence on their magnetic properties. Shape anisotropy can increase the coercivity. Enhanced anisotropy induces large magnetic coercivity, where the magnetic spins are preferentially aligned along the long axis and their reversal to the opposite direction requires higher energies than that for spheres.[12] Therefore, compared with the H_c value of the bulk Fe_3O_4 (115–150 Oe), the spherical Fe_3O_4 nanocrystallites exhibit higher values, which may be attributed to their spherical structures as observed in the Fe_3O_4 SPIONs.

Magnetic moments versus temperature (*M–T*) measurements at bias fields of 100 and 200 Oe are shown in Figs. 5(a) and 5(b). The blocking temperature is the temperature at which magnetic materials change their state from superparamagnetism to ferrimagnetism and *vice versa*. The blocking temperatures 150 and 130 K were observed for the Fe_3O_4 SPIONs and BSA-capped Fe_3O_4 SPIONs, respectively, as shown in Fig. 5(a). The increase in bias field to 200 Oe results in a decrease of blocking temperature to 120 from 130 K, as shown in Fig. 5(b). The blocking temperature, T_b, for the SPIONs is similar to T_c (Curie temperature) in bulk ferromagnetic materials. The zero field cooled (ZFC) measurements curve and field cooled (FC) curve for the SPIONs overlap at a temperature slightly higher than T_b and the magnetic susceptibility of samples obeys the Curie–Weiss law.[21,27] Zero field cooling is an experimental situation at the time of magnetization measurement when no field is applied at samples. This means that when $T < T_b$, the MNPs are ferromagnetic and when $T > T_b$, ferrimagnetism changes into paramagnetism. The blocking temperature decreases with the increase in the thickness of the MNP shell.[28–30]

In ZFC measurements, the initial field was set to zero as the sample was cooled to the lowest temperature during experiments, and the bias field was then turned on and *M–T* measurements were carried out in the temperature range from 2.5 to 300 K. In FC measurements, a bias field (*H*) of either 100 or 200 Oe was applied at 300 K and the magnetic moment was measured as the sample

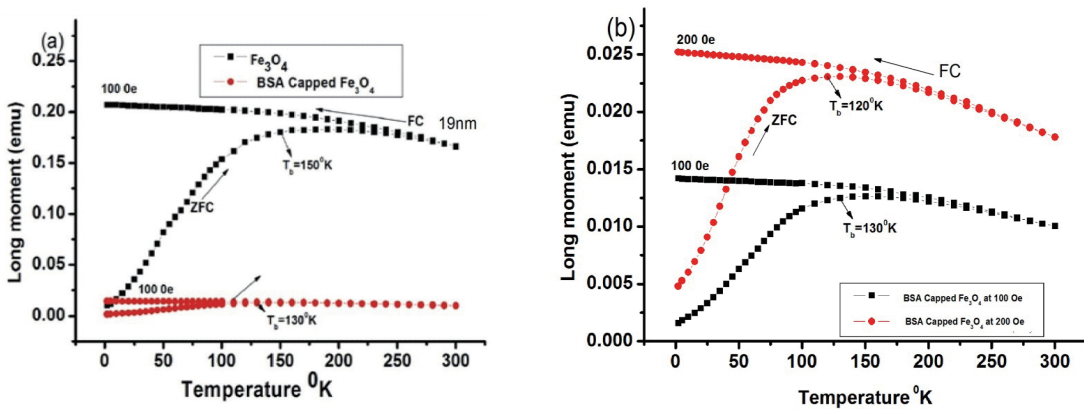

(a) (b)

Fig. 5. (Color online) (a) *M–T* curve for Fe_3O_4 and BSA-capped Fe_3O_4 at 100 Oe bias field. (b) *M–T* curve for BSA-capped Fe_3O_4 at 100 and 200 Oe bias field.

was cooled to the lowest temperature. Considering the ZFC and FC measurements, one recognizes that the splitting temperature between the ZFC and FC branches differs from the blocking temperature, which coincides with the maximum of the ZFC curve. Such behaviour is observed in randomly dipolar coupled nanomagnet systems.[31] Also, the width of the peak of the ZFC branch can be attributed to the dipolar coupling of the nanoparticles assisted owing to the distribution of the particle sizes and monodisperse nature of SPIONs as observed in TEM image (Fig. 2).

The size of the MNPs can also be estimated using ZFC data, the blocking temperature T_b was identified directly from the ZFC curve and the particle volume was obtained by the Néel–Arrhenius law: the average time (τ) taken by magnetization to flip the spin to reverse direction under the thermal fluctuations is

$$\tau = \tau_0 e^{KV/K_B T}, \tag{3}$$

where $T = T_B$, τ is the measuring time, τ_0 is a constant characteristic of the material (10^{-9}–10^{-11} s), V is the volume of nanoparticle, and K_B is the Boltzmann constant (= $1.3806505 \times 10^{-23}$ J/K). K is the anisotropy constant (energy density) for the SPIONs, which has a range of values and is dependent on the manufacturing process and shape of nanoparticles. The constant of anisotropy, K, is a source of uncertainty in particle size. After taking the logarithm of both sides at base e, and taking the experimental condition into account, the equation can be rewritten as

$$T_B = VK/25K_B. \tag{4}$$

The volume was estimated considering particles with spherical geometry and anisotropy constant ($K = 1.35 \times 10^4$ J/m^3) for the Fe_3O_4 SPIONs.[31] The particle size of the synthesized Fe_3O_4 MNPs was calculated to be 19 nm by substituting the values in Eq. (4).

The disagreement in the particle size values from *M–H* data (10 nm) and ZFC measurements data (19 nm) was due to the variation in K obtained for the MNPs. Another source of error is our assumption that the SPIONs are considered to be spherical. It is expected that SPIONs have an aspect ratio greater than 1. The Néel–Arrhenius equation for magnetization reversal from the paramagnetism state to the blocked state can be successfully utilized to predict the approximate size of SPIONs.

4. Conclusion

In the present research, Fe_3O_4 MNPs were synthesized by a modified co-precipitation technique, which yielded SPIONs with saturation magnetization of 57.54 and 11.37 emu/gm for the Fe_3O_4 SPIONs and the BSA-capped SPIONs at 10 K, respectively. *M–T* measurements showed the blocking temperatures of 150 and 130 K for the Fe_3O_4 MNPs and BSA-capped Fe_3O_4 MNPs, respectively. The variance in saturation magnetization recorded for the BSA-capped Fe_3O_4 MNPs opens up the possibility for their application in the detection of analytes in immunoassay. The average crystallite size (D) of the synthesized MNPs was estimated to be 4–6 nm, thereby making the produced magnetite material suitable for technological applications. TEM images of the MNPs showed the mean diameter of 18 ± 10 nm. *M–H* and *M–T* curve data were used separately for deduction of the particle size using the Langevin equation and Néel–Arrhenius relaxation equation, respectively. The calculated particle sizes of SPIONs were found to be 10 and 19 nm. Fe_3O_4

MNPs are an interesting system in nanotechnology applications owing to their magnetic switching behaviour between the superparamagnetic and ferromagnetic state of the system, which can be adjusted by modifying the distance between the particles.

Acknowledgements

The authors thank the Department of Science and Technology (DST), the Government of India, for creating a National SQUID Facility at the Department of Physics, ITT Delhi, New Delhi for researchers. We also thank the head and staff of the National SQUID Facility at IIT Delhi.

References

1 Z. Wang, Y. Bai, W. Wei, N. Xia, and Y. Du: Materials **6** (2013) 5690.
2 L. Bai, Y. Du, J. Peng, Y. Liu, Y. Wang, Y. Yang, and C. Wang: J. Mater. Chem. B **2**(2014) 4080.
3 D.L. Huber: Small **1** (2005) 482.
4 C. Sun, J. S. H. Lee, and M. Zhang: Adv. Drug. Deliv. Rev. **60** (2008) 1252.
5 C. Corot, P. Robert, J. M. Idee, and M. Port: Adv. Drug. Deliv. Rev. **58** (2006) 1471.
6 R. Tietze, R. Jurgons, S. Lyer, E. Schreiber, F. Wiekhorst, D. Eberbeck, H. Richter, U. Steinhoff, L. Trahms, and C. Alexiou: J. Magn. Magn. Mater. **321** (2009) 1465.
7 K. J. W. Liu, Y. Zhang, D. Chen, T. Yang, Z. P. Chen, S.Y. Pan, and N. Gu: Physicochem. Eng. Aspects **341** (2009) 33.
8 A. K. Gupta and M. Gupta: Biomater. **26** (2005) 3995.
9 E. Allard, C. Passirani, and J. P. Benoit: Biomater. **30** (2009) 2302.
10 L. Y. Zhang, H. C. Gu, and X. M. Wang: J. Magn. Magn. Mater. **311** (2007) 228.
11 H. Liu and J. Li: Iranian Polymer J. **17** (2008) 721.
12 A. H. Lu, E. L. Salabas, and F. Schuth: Angewandte Chemie. International Edition **46** (2007) 1222.
13 V. V. Mody, M. I. Nounou, and M. Bikram: Adv. Drug. Deliv. Rev. **61** (2009) 795.
14 J. W. Bulte, Y. Hoekstra, R .L Kamman, R. L. Magin, A. G. Webb, R. W. Briggs, K. G. Go, , C. E. Hulstaert, and S. Miltenyi: Magn. Reson. Med. **25** (1992) 148.
15 J. Dobson: Drug Develop. Res. **67** (2006) 55.
16 Y. M. Huh, Y. W. Jun, H.T. Song, S. Kim, J. S. Choi, J. H. Lee, S. Yoom, K. S. Kim, J. S. Shin, J. S. Suh, and J. Cheon: J. Am. Chem. Soc. **127** (2005) 12387.
17 Q. A. Pankhurst, J. Connolly, S. K. Jones, and J. Dobson: J. Phys. D-App. Phys. **36** (2003) R167.
18 V. Kumar, R. P. Singh, S. Kumar, A. Agarwal, and P. Singh: Adv. Sci. Lett. **18** (2012) 99.
19 Y. Lai, W. Yin, J. Liu, R. Xi, and J Zhan: Nanoscale Res. Lett. **5** (2010) 302.
20 N. K. Verma, K. C. Staunton, A. Satti, S. Gallagher, K. B. Ryan, T. Doody, C. McAtamney, R. MacLoughlin, P. Galvin, C. S. Burke, Y. Volkov, and Y. K. Gunko: J. Nanobiotech. **11** (2013) 1.
21 E. D. Barco, J. Asenjo, X. X. Zhang, R. Pieczynski, A. Julia, J. Tejada, R. F. Ziolo, D. Fiorani, and A. M. Testa: Chem. Mater. **13** (2001) 1487.
22 A. Curtis and C. Wilkinson: Trends Biotechnol. **19** (2001) 97.
23 O. U. Rahman, S. C. Mohapatra, and S. Ahmad: Mate. Chem. Phys. **132** (2012) 196.
24 J. M. Wilkinson: Med. Device. Technol. **14** (2003) 29.
25 S. J. Park, S. Kim, S. Lee, Z. G. Kim, K. Char, and J. Hyeon: J. Am. Chem. Soc. **122** (2000) 8581.
26 S. Ahmad, U. Ria, A. Kaushik, and J. Alam: Inorg. Organomet. Polym. **19** (2009) 355.
27 C. Petit, A. Taleb, and M. P. Pileni, Adv. Mater. **10** (1998) 259.
28 J. Chatterjee, Y. Haik, and C. J. Chen: J. Magn. Magn. Mater. **257** (2003) 113.
29 L. Fu, V. P. Dravid, and D. L. Johnson: App. Surf. Sci. **181** (2001) 173.
30 K. Runpf, P. Granitzer, P. M. Morales, P. Poelt, and M. Reissner: Nanoscale Res. Let. **7** (2012) 445.
31 J. D. Denardin, A. L. Brandl, M. Knobel, P. Panissod, A. B. Pakhomov, H. Liu, and X. X. Zhang: Phys. Rev. **65** (2002) 064422:1.